Image capture: synthesis of sensor responses from multispectral images.

Poorvi L. Vora, Michael L. Harville, Joyce E. Farrell
Hewlett-Packard Laboratories, 1501 Page Mill Road, Palo Alto, CA 94304
Phone: (415) 857-2457, Fax: (415) 857-4691
Email: { poorvi, harville, farrell }@ hpl.hp.com
Jerome D. Tietz, David H. Brainard
Dept. of Psychology, University of California at Santa Barbara
Santa Barbara, CA 93106
Phone: (805) 893-2011, Fax: (805) 893-4303
Email: {tietz, brainard }@ psych.ucsb.edu

Abstract

This paper describes the performance of an image capture simulator. The general model underlying the simulator assumes that a) the image capture device contains multiple classes of sensors with different spectral sensitivities and b) that each sensor responds linearly to light intensity over most of its operating range. We place no restrictions on the number of sensor classes, their spectral sensitivities, or their spatial arrangement. The input to the simulator is a set of narrow-band images of the scene taken with a custom-designed hyperspectral camera system. The parameters for the simulator are the number of sensor classes, the sensor spectral sensitivities, the noise statistics and number of quantization levels for each sensor class, the spatial arrangement of the sensors, and the exposure duration. The output of the simulator is the raw image data that would have been acquired by the simulated image capture device.

To test the simulator, we acquired images of the same scene both with our hyperspectral camera and with a calibrated Kodak DCS-200 digital color camera. We used the simulator to predict the DCS-200 output from the hyperspectral data. The agreement between simulated and acquired images validated the image capture response model, the spectral calibrations, and our simulator implementation. We believe the simulator will provide a useful tool for understanding the effect of varying the design parameters of an image capture device.

1 INTRODUCTION

The light sensors in many modern image capture devices (e.g. digital scanners and digital cameras) are based on Charge-Coupled Device (CCD) or Active Pixel Sensor (APS) technology. These devices are known to have linear intensity-response functions over most of their operating range [10]. By using color filters it is possible to create multiple classes of sensors with different spectral sensitivities. In the case of digital scanners, data from all sensor classes are typically provided at each image location. In the case of digital cameras, sensors from the various classes are typically interleaved, so that data from only one class is available at each image location. We refer to such devices as Color Filter Array (CFA) cameras. To produce a full multispectral image, the raw data

from a CFA camera must be processed by a demosaicing algorithm [1, 3, 2, 22, 7, 20]. How well these algorithms perform depends on the properties of the camera.

Evaluation of digital camera design parameters has received considerable attention in the recent literature [16, 13, 21, 12, 4, 5, 9, 17, 18, 11, 6]. These evaluations are based on theoretical models of image statistics and simple image quality metrics. A useful complement to the theoretical approach is to evaluate the performance of different camera designs for actual scenes. A difficulty with this approach is that it is not always feasible. This paper describes a method for constructing, testing and evaluating the performance of an image capture device simulator. The simulator, in turn, provides a means for evaluating the performance of a complete image capture device design prior to manufacture.

The simulator is based on several simplifying assumptions about the image capture device. These are a) that the optical system is linear and shift invariant, b) that the sensors respond linearly to light at varying intensities and wavelengths, and c) that the sensor noise is additive. The input to the simulator is a hyperspectral image of the scene, which provides the full spectral power distribution of the incident light at every image location. These images are acquired with a custom-built hyperspectral camera system. Given the hyperspectral image, the simulator computes the response of the image capture device using a linear response model.

2 THE LINEAR RESPONSE MODEL

The simulator is based on a linear response model. For this model, the relation between the response r and the incident light power at each image location can be expressed as

$$r = e\int_{\lambda_l}^{\lambda_h} s(\lambda)i(\lambda)d\lambda \tag{1}$$

where $s(\lambda)$ is the spectral sensitivity of the sensor, $i(\lambda)d\lambda$ the power density per unit time at wavelength λ, e the exposure duration and n a normal random variable. Typically there are three sensor types, though our simulator handles any number of sensor types. The mean and variance of n describe the dark noise and response variability of the sensor. The limits λ_l and λ_h are the wavelength limits beyond which the spectral response of the sensor is zero.

Equation (1) describes the response of the camera at each individual image location. For a CFA digital camera, the camera output is an image of sensor responses as a function of (x, y). Using equation (1), the output image obtained from the camera sensor array is:

$$r(x,y) = e\int_{\lambda_l}^{\lambda_h} s(x,y,\lambda)i(x,y,\lambda)d\lambda \; + \; n$$

where the sensor mosaic $s(x,y,\lambda)$ is the response of the sensor at position (x, y), $i(x,y,\lambda)$ is the image intensity as a function of space and wavelength as seen by the sensor array, and λ_l and λ_h are wavelength values beyond which all sensor responses are zero. In this formulation, we neglect optical blur and assume that the image seen by the sensor array is the result of an ideal linear shift-invariant imaging system whose point spread is described by a delta function. In general, optical blur must be incorporated into the image formation model. In this paper, however, we consider only images of a low-spatial frequency target (the Macbeth ColorChecker Chart) and thus neglect optical blurring.

The output image is not continuous. Rather, both the output image and sensor mosaic are defined on a two dimensional pixel grid. If the grid is regular (i.e. the distance between two sensors is identical in the horizontal and vertical directions) and one corner of the sensor array is denoted the origin, the output image at grid point

(m, n) is:

$$r(m\delta, n\delta) = e \int_{m\delta-\frac{\delta}{2}}^{m\delta+\frac{\delta}{2}} \int_{n\delta-\frac{\delta}{2}}^{n\delta+\frac{\delta}{2}} \int_{\lambda_l}^{\lambda_h} s(m\delta, n\delta, \lambda) i(x, y, \lambda) d\lambda dy dx + n \quad (2)$$

where δ is the grid spacing in either direction and we assume that $s(x, y, \lambda)$ is constant over each pixel.

It is usually not possible to provide a functional characterization of i and s, and these are often measured at discrete points in space and at discrete wavelength values. If these measurements are taken close enough that one may assume the values are constant over the area designated by a pixel and over the wavelength sampling interval, the output image at grid point (m, n) can be approximated as:

$$r(m\delta, n\delta) \approx e \sum_{k=1}^{N} s(m\delta, n\delta, \lambda_l + k\Delta_\lambda) i(m\delta, n\delta, \lambda_l + k\Delta_\lambda) \Delta_\lambda \delta^2 + n \quad (3)$$

where Δ_λ represents the wavelength sampling interval and N the total number of wavelength samples. Using discrete arguments for all of the above,

$$\mathbf{r}(m, n) \approx e \sum_{k=1}^{N} \mathbf{s}(m, n, k) \mathbf{i}(m, n, k) \Delta_\lambda \delta^2 + n \quad (4)$$

Correct calibration allows us to drop the constant $\Delta_\lambda \delta^2$ in the above sum.

We conducted extensive experiments on the Kodak DCS-200 to check whether its performance is well-described by the linear response model [14]. In general, the model provides a good description of the camera's performance. The main exception is a failure of the model near the high and low ends of the camera's operating range. These extremes were avoided in all images discussed in this paper. In addition to verifying the linear response model, we calibrated the spectral sensitivities of the red, green, and blue sensor classes employed by the DCS-200 [15]. We did this by measuring the camera's response to a series of calibrated monochromatic images. We note that the performance of a second digital camera (the Kodak DCS-420) is not well-described by the linear model, at least when it is operated with the standardly-supplied 8-bit acquistion software [14].

3 THE HYPERSPECTRAL CAMERA

The hyperspectral camera is based on a scientific grade monochrome CCD camera (Photometrics PXL, Kodak KA4200 CCD chip, 2K by 2K spatial resolution, 12 bits/pixel, cooled for low noise operation). We used the camera to acquire 31 images, each taken through a narrowband interference filter(Optical Thin Films, 400-700 nm in 10 nm steps, filter full width at half-height 8-12 nm). We varied the exposure and aperture used for each filter to bring all of the acquired images into the operating range of the camera. Exposure times ranged between 10 seconds at f2.8 (400 nm) to 0.5 seconds at f8 (610 nm).

For the initial tests presented here, we acquired hyperspectral images of the Macbeth ColorChecker Chart (MCC) illuminated by an incandescent source (Kodak 4400 Slide Projector). We also used a radiometer (Photo Research PR-650) to make direct spectral measurements of the light reflected from each of the 24 color checker squares.

3.1 Methods

To calibrate the hyperspectral camera, we used a normalization procedure [19]. We used the radiometric measurements from the white surface on the MCC to compute a single scale factor for each of the 31 narrowband

images. This scale factor was computed as follows. For each image, we found the mean camera response for a small image region centered on the white surface. We then found the scale factor necessary to equate this mean with the radiometric measurement of the white surface at the corresponding wavelength. This normalization procedure would be exactly correct were the interference filters perfectly narrowband. We attempted to characterize and correct for the finite width of the filters but did not obtain satisfactory results. We believe the reason for this is that our radiometer itself has a non-trivial passband (about 8 nm full width at half height). This finite passband makes the radiometer unsuitable for characterizing narrowband sources.

3.2 Results

To check the calibration of the hyperspectral camera, we compared the radiometric measurements of each colored surface in the MCC to the spectrum obtained from the hyperspectral images for the corresponding surface. For each surface, we computed the mean response in each component image for a small image region centered on the surface. We then scaled these means with the factors we obtained from the white surface. The results are shown in Figure 1. Each curve in the graphs compares a spectrum obtained with the radiometer (solid line) to a spectrum obtained with the hyperspectral camera (dashed line).

The agreement for the white surface (top curve, bottom right panel) is perfect since it was our calibration standard. The agreement for most other surfaces is also very good. For a few surfaces there is a systematic bias between the two spectra. We attribute this bias to geometric imaging factors and plan to assess it more carefully in the future. There is also a problem with the 650 nm component image, which can be seen in some curves as a bump in the hyperspectral camera spectrum. This suggests that there is a problem with our 650 nm filter. We plan to purchase a replacement filter to test this hypothesis.

3.3 Discussion

The preliminary test reported here demonstrates the feasibility of acquiring hyperspectral images with our system. Our design does have some limitations. The most major of these is that we can only acquire images of stationary scenes, since we must acquire the component images sequentially. A more minor limitation is that we must calibrate our images to a spectral standard. This is not, however, difficult given that we are already constrained to work with stationary scenes. It is trivial to insert a reference white into each scene and to acquire a radiometric image of it.

The next steps in the development of this system are to perform measurements to understand how much the spectral sensitivity of our system varies across each component image, to develop methods for precise alignment of the component images, and to characterize the multispectral point spread function of the hyperspectral camera.

4 DESCRIPTION OF THE SIMULATOR

Fig. 2 shows a block diagram of the simulator. The input consists of a set of images which together represent an approximation of the intensity incident on the camera lens as a function of space and wavelength. At present, the input is a set of 31 images taken with the hyperspectral camera system described in section 3. The 31 images each represent a spatial distribution of the incident intensity over a narrow range of wavelength values. The simulator can also take a different representation of the input, for example a set of images each of which represents the spatial distribution of coefficients with respect to a basis set of principal components of a database of reflective spectra.

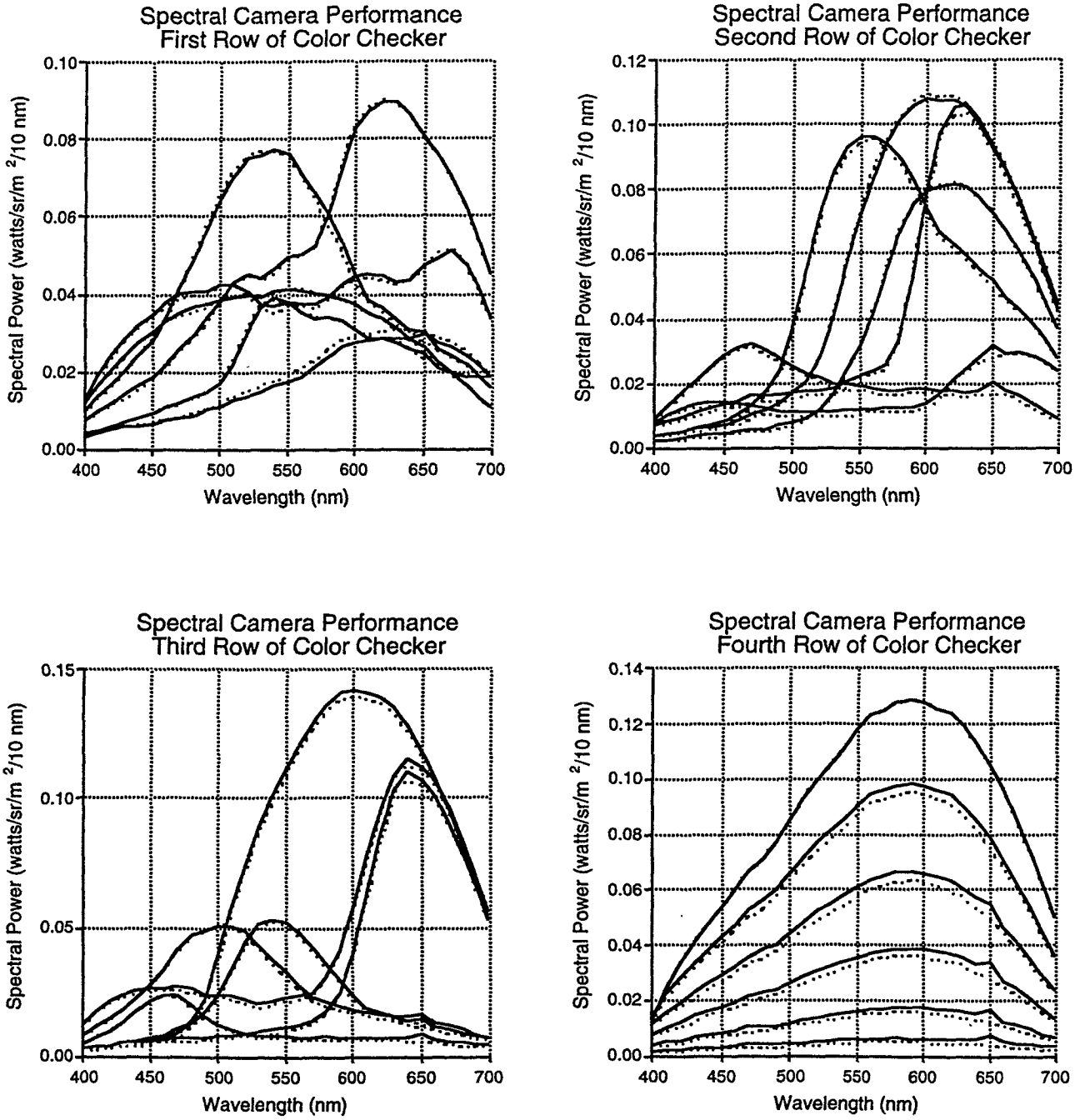

Figure 1: Verification of hyperspectral camera performance: The dashed line represents the radiometric data and the solid line represents the spectral data predicted by the hyperspectral camera

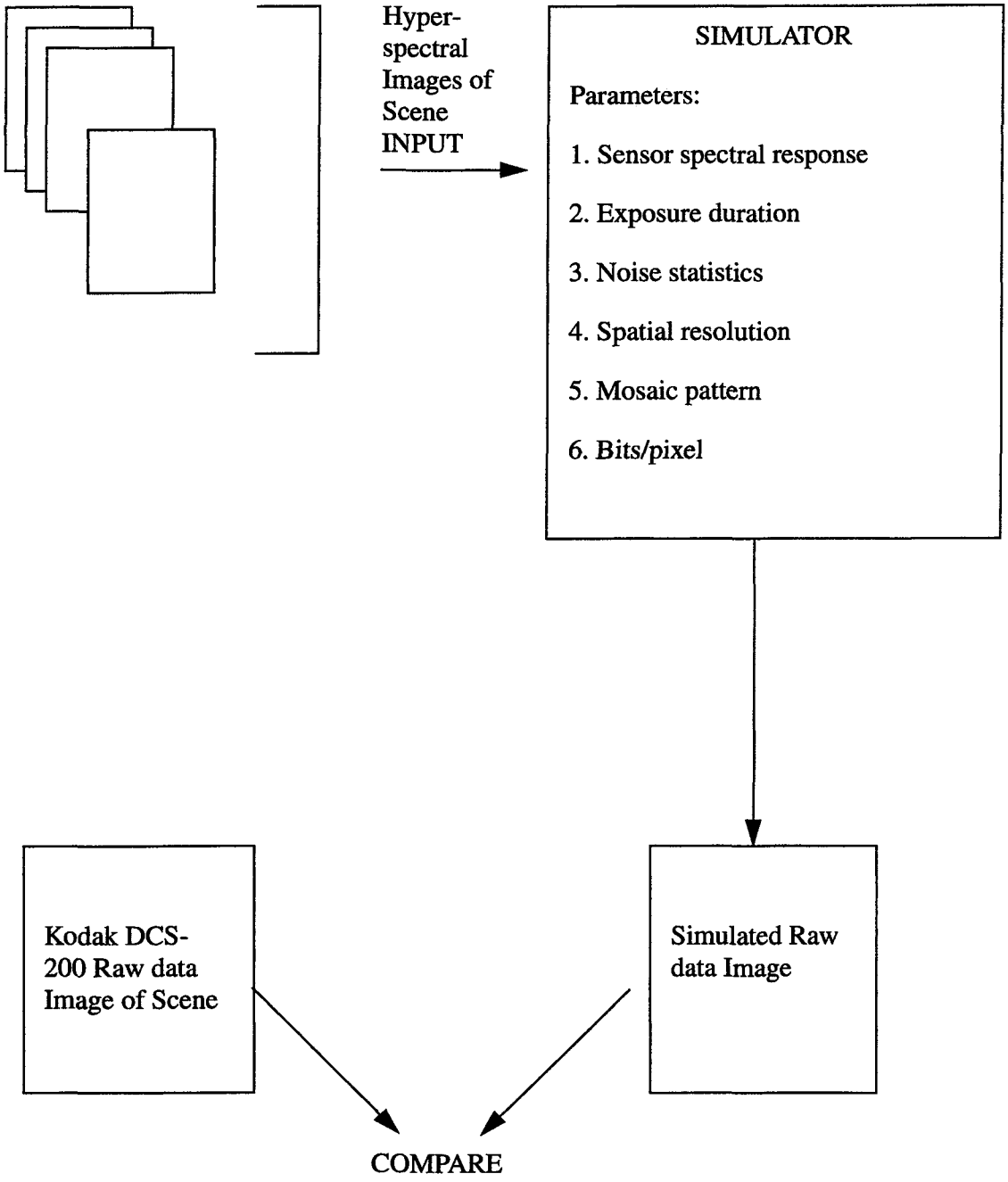

Figure 2: Block Diagram of Simulator

The parameters of the simulator are:

1. the sensor spectral sensitivities as a function of wavelength, sampled at the same rate as the representation of the input (or represented in terms of the same basis vectors as the input)
2. the exposure time
3. the noise statistics (mean and variance)
4. the spatial resolution
5. the mosaic pattern
6. the number of bits per pixel of the camera sensors

Our simulator implementation uses equation 4 to compute the simulated output image. A final step of the simulation, not described by equation 4 is to quantize the simulated output to the same number of bits as the simulated device.

The output raw data image of the simulator may be directly compared with the camera image for numerical verification. For visual quality judgements, we need to demosaic and color correct the outputs of the DCS-200 and the simulator and then compare the color images.

5 VERIFICATION RESULTS

This section describes the experiments performed to verify the accuracy of the simulator for color patches. The performance of the simulator was verified as follows. The DCS-200 was used to take pictures of the Macbeth ColorChecker Chart (MCC) in a laboratory illuminated by an incandescent source (Kodak 4400 Slide Projector) at different exposure settings: 1/8, 1/15, 1/30, 1/60 and 1/125 seconds. The hyperspectral camera system was also used to take the 31 hyperspectral images of the same chart in the same conditions, as described in section 3. The 31 images, the estimated DCS-200 spectral sensitivities, the exposure durations, the measured noise statistics and the bits per pixel value (8) of the DCS-200 were used to generate simulated images. The simulated images were compared both numerically and visually.

Figure 3 is a scatter plot of the real vs. simulated R, G, B values over all the shutter speeds studied in the experiment. It is clear that the agreement between real and simulated values is good.

Table 1 lists the numerical error statistics of R, G, and B values averaged over the centre of each patch in both real and simulated images. Since the DCS-200 is an 8-bit camera, the numerical response values range between 0 and 255. The values in the table are computed from response values on this scale.

For purposes of comparison, the spatial variation in a dark noise image taken with the DCS-200 has a root mean square value of about 0.9. Linearity tests for this camera have shown that the root mean square value of the variation from linearity is 1.45 [14]. Furthermore, the correspondence between predicted and empirical sensor values is consistent across exposure settings, supporting our assumption of linearity with respect to exposure duration (an assumption implicit in equation 4).

We visually compared the predicted and empirical sensor data after after processing the data with a simple demosaicing routine based on bilinear interpolation. (The complexity of the demosaicing routine is not expected to make a difference to visual quality, as the images consist of large color patches.) The real and simulated images have very similar appearances.

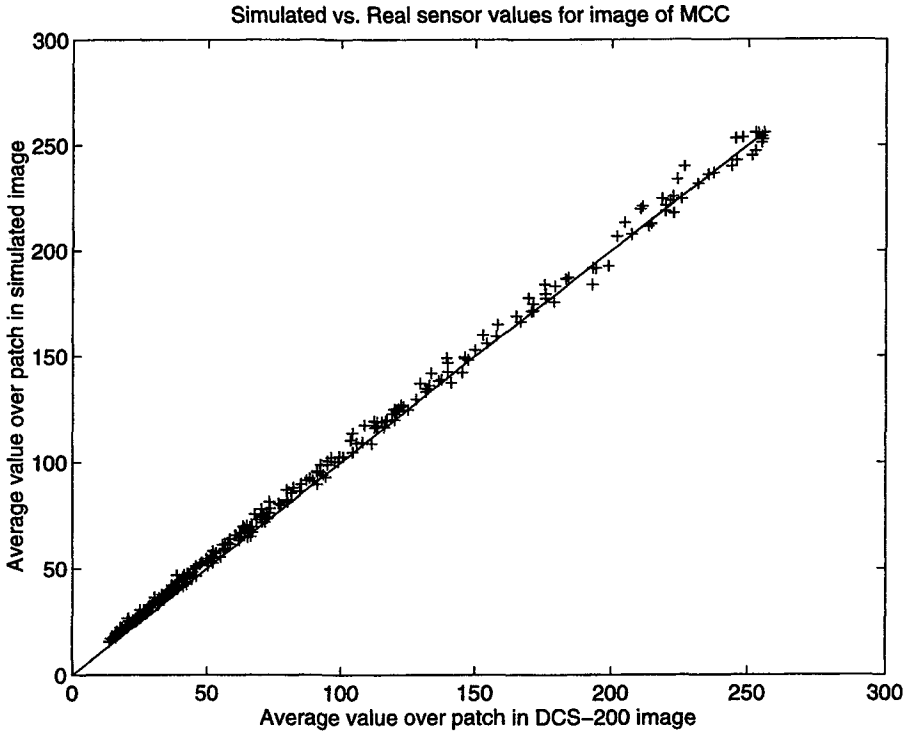

Figure 3: Scatter plot of MCC color simulation

Table 1: Statistics of Estimation Error for MCC - DCS-200.

Exposure Setting in sec.	Mean of Absolute Error	Mean of Absolute % Error	RMS Error	Maximum Absolute Error	Maximum Absolute % Error
$\frac{1}{8}$	1.49	1.22	2.59	9.07	13.23
$\frac{1}{15}$	3.18	4.03	4.11	9.64	30.99
$\frac{1}{30}$	4.96	7.66	5.43	13.21	24.13
$\frac{1}{60}$	3.47	9.39	3.66	6.75	26.19
$\frac{1}{125}$	1.85	7.22	1.96	3.04	15.16

6 CONCLUSIONS AND FUTURE POSSIBILITIES

The use of a linear model is appropriate for the calibration, modelling and simulation of the sensor responses of color filter array cameras. The color fidelity of the output of the simulator is good for a wide range of exposure settings. In the future we will incorporate a model for the optical system to simulate the effects of lens blur. The simulation of spatial effects (including the effect of a lens blur that may vary as a function of position with respect to center-field and wavelength, inter-sensor charge leakage and the mosaic pattern) on the visual quality of an image will be verified by using calibrated hyperspectral input images of scenes with richer spatial variation.

References

[1] Brainard, D. H., *Bayesian method for Reconstructing Color Images from Trichromatic Samples*, IS&T, 47th Annual Conference, pp. 375-380, 1994.

[2] Cok, D. R., *Signal processing method and apparatus for sampled image signals*, United States patent 4630307, 1986

[3] Cok, D. R., *Reconstruction of CCD Images Using Template Matching*, IS&T, 47th Annual Conference, pp. 380-385, 1994.

[4] Engeldrum, P. G., *Almost Color Mixture Functions*, Journal of Imaging Technology, Vol. 14, No. 4, pp. 108-110, Aug. 1988.

[5] Engeldrum, P. G., 'Color Scanner Colorimetric Design Requirements' *Proceedings of IS&T/SPIE Symposium on Electronic Imaging: Science and Technology*, San Jose, CA, USA, Jan. 31 - Feb. 4, 1993.

[6] Engelhardt, K. and Seitz, P., *Optimum color filters for CCD digital cameras*, Optical Engineering, vol. 32, no. 16, pp. 3015-3023, Jun. 1993.

[7] Freeman, W., *Method and apparatus for reconstructing missing color samples*, United States Patent 4663655, 1987.

[8] Hubel, P. M., Sherman, D. and Farrell, J. E., *A Comparison of Methods of Sensor Spectral Sensitivity Estimation*, Proc., IS&T/SID 2nd. Color Imaging Conference: Color Science, Systems and Applications, pp. 45:48, 1994.

[9] Iwan, L. S., *Calibration of Color Input Scanners for Accurate Color Reproduction*, Proc., SPIE, 43rd Annual Conference, Rochester, NY, May 22-25, 1990.

[10] Lomheim, T. S. and Kalman, L. S., *Analytical Modeling and Digital Simulation of Scanning Charge-Coupled Device Imaging Systems* in Electro-Optical Displays ed. Karim, M. A., Marcel Dekker, 1992.

[11] Neugebauer, H. E. J., *Quality Factor for Filters Whose Spectral Transmittances are Different from Color Mixture Curves, and its Application to Color Photography*, Journal of the Optical Society of America, Vol. 46, No. 10, pp 821-824, Oct 1956.

[12] Sharma, G. and Trussell, H. J., *Figures of merit for color scanners and cameras*, in review, IEEE Trans. Image Proc.

[13] Trussell, H. J., Sharma, G., Chen, P., and Rajala, S. A., *Comparison of measures of goodness of sets of color scanning filters*, Proceedings IEEE Multi-dimensional Signal Processing Workshop, Belize, Mar. 4-6, 1996.

[14] Vora, P. L., Farrell, J. E., Tietz, J. D., Brainard, D. H., *Digital color cameras - 1 - Response models*, Hewlett-Packard Company, Technical Report.

[15] Vora, P. L., Farrell, J. E., Tietz, J. D., Brainard, D. H., *Digital color cameras - 2 - Spectral response*, Hewlett-Packard Company, Technical Report.

[16] Vora, P. L., and Trussell, H. J., *Measure of Goodness of a Set of Colour Scanning Filters*, Journal of the Optical Society of America - A, Vol. 10, No. 7, July 1993.

[17] Vrhel, M. J., and Trussell, H. J., *Filter Considerations in Color Correction*, IEEE Transactions on Image Processing, Vol. 3, No. 2, pp. 147-161, Mar. 1994.

[18] Vrhel, M. J., and Trussell, H. J., *Optimal Color Filters in the Presence of Noise*, IEEE Transactions on Image Processing, Vol. 4, No. 6, Jun. 1995.

[19] Webster, M., personal communication, 1996.

[20] Wober, M. A. and Soini, R. *Method and apparatus for recovering image data through the use of a color test pattern*, United States Patent 5475769, 1995.

[21] Wolski, M., Allebach, J. P., Bouman, C. A. and Walowit, E., *Optimization of sensor response functions for colorimetry of reflective and emissive objects*, IEEE Trans. Image Proc., vol5, no. 3, pp. 507-517, Mar. 1996.

[22] *Programmer's Reference Manual Models: DCS200ci, DCS200mi, DCS200c, DCS200m.* Eastman Kodak Company, December 1992.

[23] *MATLAB High-Performance Numeric Computation and Visualization Software, Reference Guide*, The MathWorks, Inc., 1992.